

Thermally activated charge carriers and mid-infrared optical excitations in quarter-filled CDW systems

I. Kupčić

Department of Physics, Faculty of Science, University of Zagreb, POB 331, HR-10 002 Zagreb, Croatia

The optical properties of the quarter-filled single-band CDW systems have been reexamined in the model with the electron-phonon coupling related to the variations of electron site energies. It appears that the indirect, electron-mediated coupling between phase phonons and external electromagnetic fields vanishes for symmetry reasons, at variance with the infrared selection rules used in the generally accepted microscopic theory. It is shown that the phase phonon modes and the electric fields couple directly, with the coupling constant proportional to the magnitude of the charge-density wave. The single-particle contributions to the optical conductivity tensor are determined for the ordered CDW state and the related weakly doped metallic state by means of the Bethe-Salpeter equations for elementary electron-hole excitations. It turns out that this gauge-invariant approach establishes a clear connection between the effective numbers of residual, thermally activated and bound charge carriers. Finally, the relation between these numbers and the activation energy of dc conductivity and the optical CDW gap scale is explained in the way consistent with the conductivity sum rules.

PACS numbers: 71.45.Lr, 78.30.-j, 78.20.Bh

Keywords: CDW systems, optical properties, Bethe-Salpeter equations, single-particle excitations

I. INTRODUCTION

The electrodynamic of low-dimensional multiband systems in which strong correlations responsible for formation of localized electronic states coexist with correlations responsible for charge-density-wave ordering (CDW) still attract great attention. The vanadium chain compound BaVS_3 is a typical example of such (magnetic) metals with the commensurate CDW instability [1, 2, 3, 4]. In this system, basic electrodynamic properties are related to one wide band, while magnetic anomalies are associated with more or less localized states in two narrow bands. The relations between the mid-infrared (MIR) energy scales, measured at temperatures below the critical CDW temperature, the activation energies of transport coefficients and the related effective numbers of conduction electrons are not entirely clear [3]. In order to explain these relations in simple physical terms, one needs, in the first place, a precise description of the CDW coherence effects in the quarter-filled wide band. This problem that is still not completely solved for the single-band case is in the focus of this work.

The previous theoretical work [5, 6, 7, 8, 9, 10, 11, 12, 13, 14, 15, 16, 17, 18] on the electrodynamic of the single-band CDW systems followed two basic routes. First, the collective contributions have been studied to explain the low- and zero-temperature properties of the incommensurate CDW systems, with the emphasis on the non-linear conductivity regime [12, 13]. The main controversies characterizing early theoretical investigations are resolved using accurate symmetry analyses, with a particular care devoted to the local field effects [14]. The principal physical problem in these analyses is that the coupling between infrared-active collective modes and external electromagnetic fields is shown as a simple function of the single-particle (interband) polarizability [5, 7, 13, 14],

which implies the indirect electron-mediated, rather than the direct, photon-phase phonon coupling. The high (MIR) frequency analyses [17, 18], on the other hand, were focussed on the precise description of the single-particle excitations, in particular on the rigorous treatment of the square-root singularity in the optical conductivity spectra at $\hbar\omega = 2\Delta$. It is shown that the controversies related to the high-frequency optical spectra usually reflect the incorrect treatment of the diamagnetic current in the transverse response approaches, and, consequently, can be easily avoided using the longitudinal response theory [19].

In this article, we consider a quarter-filled single-band CDW system and a related tetramerized metallic system in which all non-retarded short-range interactions are neglected, and all coherence effects in the correlation functions associated with the retarded, phonon-mediated interactions are treated exactly through the known analytical form of the current vertices and the inverse effective-mass tensor. Using this exactly solvable model, we re-examine several textbook results [5, 6, 7, 8] for the dc and optical conductivity of commensurate CDW systems. The analysis is however limited by the use of several approximations. We consider a Holstein-like electron-phonon coupling in which the coupling constant is independent of the electron wave vectors. Being interested in the optical conductivity spectra obtained by the reflectivity measurements, which are characterized by a relatively poor resolution in the low-frequency part of the spectra, we approximate the total optical conductivity by the sum of the collective and single-particle contributions, with the local field effects included only in the collective term. In the numerical analysis of the single-particle term, we consider the simplest case in which two relaxation rates are assumed to be independent of frequency and temperature. Finally, the commensurability

(Umklapp) effects are present in the model through the shift of the phase phonon frequency to a finite value and through the commensurate photon-phonon coupling (see Sec. 5).

The article is organized as follows. In Sec. 2, the band dispersions of the tetramerized CDW case are briefly discussed. In Secs. 3 and 4.1, we consider the electron-hole excitations in the two-band version of the model in which the Umklapp effects are neglected. The emphasis is on the clear identification of the effectively free and effectively bound charge carriers in the underdamped regime (the interband damping energy is small in comparison with the CDW gap), their relation to both the activation energy of dc conductivity and the MIR scale in the optical conductivity. The brief discussion of the optical conductivity spectra in the overdamped regime, tentatively related to the hybridizations/interactions with localized electronic states, is given in Sec. 4.2. In Sec. 5, the infrared selection rules for the collective modes in the commensurate CDW systems are discussed in some detail. It is shown that the (interband) electron-mediated photon-phase phonon coupling vanishes for symmetry reasons, and that the direct coupling is proportional to the magnitude of the charge-density wave.

II. TETRAMERIZED CDW CASE

A. Bloch energies

The starting point of the present analysis is the Q1D tetramerized model in which the electron-phonon coupling is formulated in terms of the displacement vector

$$\mathbf{u}_i = \mathbf{u}_{\varphi i} + \mathbf{u}_{A i} = \sqrt{\frac{2}{N}} \sum_{\mathbf{q} \approx 0} e^{i\mathbf{q} \cdot \mathbf{r}_i} [\mathbf{u}_{\varphi \mathbf{q}} \cos \phi_i - \mathbf{u}_{A \mathbf{q}} \sin \phi_i], \quad (1)$$

where $\phi_i = \mathbf{Q} \cdot \mathbf{r}_i - \phi$, \mathbf{r}_i is the position of an atom and ϕ is an arbitrary phase. Two Fourier components of interest, $\mathbf{u}_{A \mathbf{q}}$ and $\mathbf{u}_{\varphi \mathbf{q}}$, are functions of two ordinary components of the wave vectors $\mathbf{q} \pm \mathbf{Q}$, as follows $\mathbf{u}_{A \mathbf{q}} = (1/\sqrt{2})[\mathbf{u}_{\mathbf{q}+\mathbf{Q}} + \mathbf{u}_{\mathbf{q}-\mathbf{Q}}]$ and $\mathbf{u}_{\varphi \mathbf{q}} = (i/\sqrt{2})[\mathbf{u}_{\mathbf{q}+\mathbf{Q}} - \mathbf{u}_{\mathbf{q}-\mathbf{Q}}]$. $\mathbf{u}_{A i}$ and $\mathbf{u}_{\varphi i}$ correspond to two similar lattice deformations which phase is shifted by $\pi/2$ and which frequency is expected to be strongly renormalized for low enough temperatures and for the band filling close to the quarter filling (evidently, $\mathbf{u}_{\lambda \mathbf{q}} = \mathbf{u}_{\lambda - \mathbf{q}}^\dagger$, with $\lambda = A, \varphi$ being the phonon branch index). $\mathbf{Q} = (0.5\pi/a, Q_y)$ is the nesting vector of the Fermi surface of the quarter-filled (CDW) case, or the tetramerization vector in a general (metallic) case. The related variations of the electron site energies (see Fig. 1), which are assumed to be the main mechanism of the electron-phonon coupling here, are

$$\begin{aligned} V(\mathbf{r}_i) &= V_\varphi(\mathbf{r}_i) + V_A(\mathbf{r}_i) \\ &= \frac{2g}{\sqrt{N}} \sum_{\mathbf{q} \approx 0} e^{i\mathbf{q} \cdot \mathbf{r}_i} [u_{\varphi \mathbf{q}} \sin \phi_i + u_{A \mathbf{q}} \cos \phi_i]. \quad (2) \end{aligned}$$

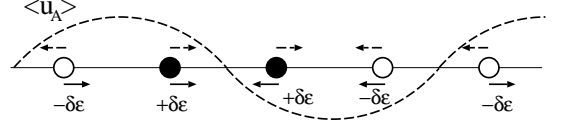


FIG. 1: Variations of the electron site energies ($-\delta\varepsilon$, $+\delta\varepsilon$, $+\delta\varepsilon$, $-\delta\varepsilon$) induced by the periodic (tetramerization) lattice distortion $u_{A\mathbf{q}} \rightarrow \delta_{\mathbf{q},0}\langle u_A \rangle$ and $\phi = \pi/4$ in Eq. (1). The solid and dashed arrows illustrate the Raman-active and infrared-active $\mathbf{q} \approx 0$ modes. The effective charges of the white and the black ions are $+q$ and $-q$, respectively. Here $\delta\varepsilon = \sqrt{2}\Delta$ and $q = q_c/\sqrt{2}$.

g is the electron-phonon coupling constant. The direct inspection of Fig. 1 shows that the periodic lattice distortion associated with the replacement $u_{A\mathbf{q}} \rightarrow \delta_{\mathbf{q},0}\langle u_A \rangle + u_{A\mathbf{q}}$ leads to the charge transfer of the magnitude q_c (determined in Sec. 5) modulated by the wave vector \mathbf{Q} . This lattice distortion makes $u_{A\mathbf{q}}$ and $u_{\varphi \mathbf{q}}$ to be the long wavelength phonon modes which are, respectively, Raman and infrared active. The other phonon modes are taken into account later in Sec. 3, and are treated on the same footing with the static disorder.

The CDW instability of the quarter-filled Q1D electronic systems in the case in which the disorder is absent and the electron-phonon coupling g is independent of the electron wave vectors is described by the well-known textbook expressions (see Eqs. (A1)–(A10) in Appendix). The commensurability effects enter in the theory through the ϕ dependent (Umklapp) contributions in the Bloch energies $E_L(\mathbf{k})$. For example, in the 1D limit ($t_b \rightarrow 0$), the four Bloch energies $E_L(\mathbf{k})$ are ($L = C, \underline{C}, V, \underline{V}$ is the band index)

$$\begin{aligned} E_{C, \underline{C}}(\mathbf{k}) &= -\sqrt{2t_a^2 + 2\Delta^2 \pm 2t(\mathbf{k})}, \\ E_{V, \underline{V}}(\mathbf{k}) &= \sqrt{2t_a^2 + 2\Delta^2 \mp 2t(\mathbf{k})}, \\ t(\mathbf{k}) &= \sqrt{2\Delta^2 t_a^2 + t_a^4 \cos^2 2k_x a + \Delta^4 \cos^2 2\phi}, \end{aligned} \quad (3)$$

with t_a and t_b being the bond energies in the highly conducting direction and in the perpendicular direction, respectively, and $\Delta = g\langle u_A \rangle/\sqrt{N}$ is the magnitude of the order parameter. When Δ is small enough, the dispersions of two lowest bands can be approximated by

$$E_{C, \underline{C}}(\mathbf{k}) = \tilde{\varepsilon}(\mathbf{k}) \mp \sqrt{\tilde{\varepsilon}^2(\mathbf{k}) - \varepsilon_c(\mathbf{k})\varepsilon_{\underline{c}}(\mathbf{k}) - U(\mathbf{k})}. \quad (4)$$

Here $\varepsilon_c(\mathbf{k}) = \varepsilon(\mathbf{k}) = -\sum_{\alpha} 2t_{\alpha} \cos k_{\alpha} a_{\alpha}$ and $\varepsilon_{\underline{c}}(\mathbf{k}) = |\varepsilon(\mathbf{k} + \mathbf{Q})|$ are two relevant bare dispersions, and $2\tilde{\varepsilon}(\mathbf{k}) = \varepsilon_c(\mathbf{k}) + \varepsilon_{\underline{c}}(\mathbf{k})$, $\tilde{\varepsilon}(\mathbf{k}) \approx \bar{\varepsilon}(\mathbf{k}) + \Delta^2/(2\bar{\varepsilon}(\mathbf{k}))$ are useful abbreviations. The Umklapp processes are represented in the dispersions (4) through

$$U(\mathbf{k}) \approx \alpha \left(1 + \frac{\Delta^2}{4\tilde{\varepsilon}^2(\mathbf{k})} \right) \frac{2\Delta^4 - \delta^4(\mathbf{k}) - (\delta^*(\mathbf{k}))^4}{4\tilde{\varepsilon}^2(\mathbf{k})}, \quad (5)$$

with $\delta(\mathbf{k}) = \Delta \exp\{i\phi(\mathbf{k})\}$, $\phi(\mathbf{k}) = \text{sgn}(k_x)\phi$ and $\alpha = 1$. The quarter-filled $\alpha = 0$ limit of Eq. (4) with $\tilde{\varepsilon}^2(\mathbf{k}) \approx$

$\bar{\varepsilon}^2(\mathbf{k}) + \Delta^2$ corresponds to the usual Peierls model which electrodynamic properties will be studied in more detail in Secs. 3 and 4.

B. Optical conductivity in pure CDW systems

In the present context, the main effect of the Umklapp processes is to shift the renormalized frequency $\omega_{\varphi 0}$ of the $\mathbf{q} = q_x \hat{e}_x = 0$ phase phonon mode from zero to a finite value [5]. Together with other pinning mechanisms, this gives the collective contribution to the optical conductivity of the form (see Fig. 2(a))

$$\sigma_{xx}^{\varphi}(\omega) = \frac{e^2 n}{m^*} \frac{i\omega}{\omega(\omega + i\gamma_{\varphi\mathbf{q}}) - \omega_{\varphi\mathbf{q}}^2}, \quad (6)$$

with m^* being the collective mode effective mass. In the pure case, where the scattering of electrons on both the disorder and the phonon modes is neglected, $\omega_{\varphi\mathbf{q}}$ and $\gamma_{\varphi\mathbf{q}}$ in Eq. (6) are the solutions of the usual functional integral approach [10], or the solutions of the Dyson equation shown in Fig. 2(b) [5, 6, 7]. The structure of m^* and $\omega_{\varphi\mathbf{q}}$ is discussed in more detail in Sec. 5 and Appendix.

The related single-particle contribution to the optical conductivity (Fig. 2(c)) is given, for example, by the gauge-invariant expression

$$\sigma_{\alpha\alpha}^{\text{sp}}(\omega) = \frac{i\omega}{q_{\alpha}^2} \chi_{1,1}(q_{\alpha}, \omega) = -i\omega\alpha(q_{\alpha}, \omega) \quad (7)$$

obtained by means of the longitudinal response theory [20] (the left-hand side of Fig. 2(c), with $\mathbf{q} = q_{\alpha} \hat{e}_{\alpha}$). $\chi_{1,1}(q_{\alpha}, \omega)$ is the sum of the intra- and interband charge-charge correlation functions defined in Appendix, and $\alpha(q_{\alpha}, \omega)$ is the related polarizability.

III. BETHE-SALPETER EQUATIONS

We take the collective mode contribution (6) aside and continue with the examination of the (single-particle) electrodynamic properties of the $\alpha = 0$ two-band model of Eqs. (4),(5). The Bloch energies are

$$E_{C,\underline{C}}(\mathbf{k}) = \bar{\varepsilon}(\mathbf{k}) \mp \sqrt{(1/4)\bar{\varepsilon}_{\underline{c}}^2(\mathbf{k}) + \Delta^2}, \quad (8)$$

with $\bar{\varepsilon}_{\underline{c}}(\mathbf{k}) = \varepsilon_{\underline{c}}(\mathbf{k}) - \varepsilon_c(\mathbf{k})$. To make the analysis more general, we consider two regimes of the two-band model close to the quarter filling in which an important role is played by thermally activated electrons in both transport and optical properties. The first regime corresponds to the ordered CDW state considered above, while the second regime is associated with the metallic state, where the doubled Fermi wave vector is $2k_{\text{F}} \neq Q_x = 0.5\pi/a$.

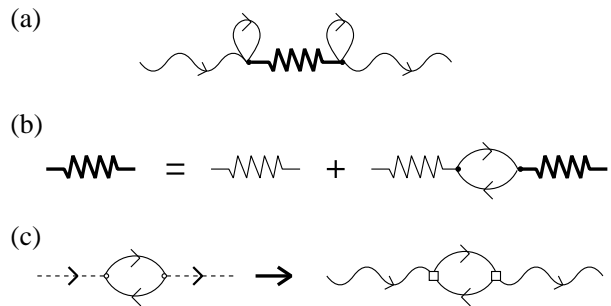


FIG. 2: The collective (a) and single-particle (c) contributions to the optical conductivity in pure regime of the present CDW model. The solid lines are the electron propagators and the zigzag lines are the phonon propagators. The open circles, the open squares and the full circles represent the charge vertices, the current vertices and the electron-phonon coupling constants, respectively. The dashed line is the external scalar field $V^{\text{ext}}(\mathbf{q}, \omega)$ and the wavy line is the related electric field (see Eq. (13)). (b) The Dyson equation for the phonon Green functions. The phonon self-energy is given by the expression (A10) in Appendix.

A. Relaxation processes on the (quasi)static disorder

Having in mind the known structure of the current vertices related to the bands (8) [21], or, alternatively, calculating the long wavelength charge vertices (29), we can make the generalization of the optical conductivity (7) to the case in which the (quasi)static disorder is present. This can be easily done by using the longitudinal equation-of-motion approach [20, 22], because this approach treats the (intraband) charge continuity equation in a natural way (the calculation is more complicated in the transverse response theory [23]). The result (Eqs. (22) and (25)) is equal to Eq. (7) with the adiabatic term η in the charge-charge correlation functions replaced by two phenomenological damping energies $\hbar\Gamma_{\alpha}^{\text{intra}}$ and $\hbar\Gamma_{\alpha}^{\text{inter}}$.

The longitudinal equation-of-motion approach is one example of the calculations which describe the elementary electron-hole excitations in the effective single-particle multiband models in the gauge-invariant way. The Bethe-Salpeter approach, described below, is another example. In both cases, the elementary excitations are represented by the Matsubara electron-hole propagator

$$\mathcal{D}^{LL'}(\mathbf{k}, \mathbf{k}_+, \mathbf{k}'_+, \mathbf{k}', \tau) = \sum_n \mathcal{D}_{(2n)}^{LL'}(\mathbf{k}, \mathbf{k}_+, \mathbf{k}'_+, \mathbf{k}', \tau),$$

where

$$\begin{aligned} \mathcal{D}_{(n)}^{LL'}(\mathbf{k}, \mathbf{k}_+, \mathbf{k}'_+, \mathbf{k}', \tau) &= \frac{(-1)^{n+1}}{\hbar^n n!} \int_0^{\beta\hbar} d\tau_1 \dots \int_0^{\beta\hbar} d\tau_n \\ &\times \langle T_{\tau} [H_1'(\tau_1) \dots H_1'(\tau_n) c_{L\mathbf{k}\sigma}^{\dagger}(\tau) c_{L'\mathbf{k}+\mathbf{q}\sigma}(\tau) \\ &\times c_{L'\mathbf{k}'+\mathbf{q}\sigma}^{\dagger}(0) c_{L\mathbf{k}'\sigma}(0)] \rangle \end{aligned} \quad (9)$$

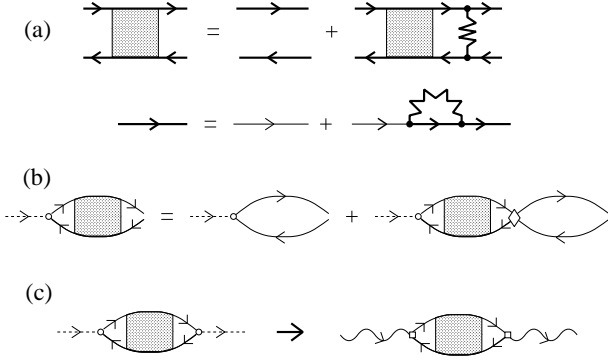


FIG. 3: (a) The Bethe–Salpeter equations. (b) The related self-consistent equations for the induced densities $\delta n^{LL'}(\mathbf{k}, \omega)$. The diamond represents the electron-hole self-energy. (c) The generalization of Fig. 2(c).

and $\mathbf{k}_+ = \mathbf{k} + \mathbf{q}$. Here H'_1 describes the scattering of conduction electrons on the (quasi)static disorder. Using this approach, it is possible to treat the relaxation processes on impurities, on lattice imperfections, and even on soft phonons. The hybridization with other (uncorrelated) bands can also be studied in this way.

B. Relaxation processes on phonons

In the presence of inelastic electron scattering processes on phonon modes, or other boson modes in general, one can use a similar longitudinal diagrammatic approach based on the self-consistent Bethe–Salpeter equations for

$$\Phi^{LL'}(\mathbf{k}; i\omega_n) \equiv \Phi^{LL'}(\mathbf{k}, \mathbf{k}_+, \mathbf{k}'_+, \mathbf{k}', i\omega_n, i\omega_{n+})$$

($i\omega_{n+} = i\omega_n + i\nu_n$). In this case H'_1 in Eq. (9) represents the electron-phonon Hamiltonian (A4) with the phonon wave vector \mathbf{q}' running over the entire Brillouin zone and the phonon branch index λ running over all (elastic and inelastic) scattering channels. $\Phi^{LL'}(\mathbf{k}; i\omega_n)$ is defined by the Fourier transform of $\mathcal{D}^{LL'}(\mathbf{k}, \mathbf{k}_+, \mathbf{k}'_+, \mathbf{k}', \tau)$,

$$\begin{aligned} \mathcal{D}^{LL'}(\mathbf{k}, \mathbf{k}_+, \mathbf{k}'_+, \mathbf{k}', i\nu_n) \\ = (\hbar/\beta) \sum_{i\omega_n} \Phi^{LL'}(\mathbf{k}, \mathbf{k}_+, \mathbf{k}'_+, \mathbf{k}', i\omega_n, i\omega_{n+}). \end{aligned} \quad (10)$$

For temperatures and dopings not too close to the critical values characterizing the CDW metal-to-insulator phase transition, the interband electron-phonon coupling in H'_1 can be neglected (notice that beyond this approximation one needs four band indices in the electron-hole propagator (9)). Now, for $G_\lambda^{LL}(\mathbf{k} + \mathbf{q}', \mathbf{k}) \approx \sqrt{\hbar/(2M\omega_{\lambda\mathbf{q}'})} \times gg_\lambda^{LL}(\mathbf{k} + \mathbf{q}', \mathbf{k})$ and $|G_\lambda^{LL}(\mathbf{k} + \mathbf{q}', \mathbf{k})|^2 \approx |G_\lambda(\mathbf{q}')|^2$, the Bethe–Salpeter equations [24] take the

form (see Fig. 3(a))

$$\begin{aligned} [i\hbar\nu_n + E_{LL'}(\mathbf{k}, \mathbf{k}_+) + \Sigma_L(\mathbf{k}, i\omega_n) - \Sigma_{L'}(\mathbf{k}_+, i\omega_{n+})] \\ \times \Phi^{LL'}(\mathbf{k}; i\omega_n) = \frac{1}{\hbar} [\mathcal{G}_L(\mathbf{k}, i\omega_n) - \mathcal{G}_{L'}(\mathbf{k}_+, i\omega_{n+})] \\ \times \left\{ \delta_{\mathbf{k}, \mathbf{k}'} - \frac{1}{\beta\hbar} \sum_{\lambda\mathbf{q}'i\nu_m} \frac{|G_\lambda(\mathbf{q}')|^2}{N} \mathcal{D}_\lambda(\mathbf{q}', i\nu_m) \right. \\ \left. \times \Phi^{LL'}(\mathbf{k} + \mathbf{q}'; i\omega_n + i\nu_m) \right\}, \quad (11) \end{aligned}$$

in obvious notation ($E_{LL'}(\mathbf{k}, \mathbf{k}_+) = E_L(\mathbf{k}) - E_{L'}(\mathbf{k}_+)$ is the electron-hole-pair energy). In the intraband channel, these equations transform into two coupled equations, one is the charge continuity equation and the other is the transport equation. These two equations have to be solved self-consistently. For this purpose, we retain in Eqs. (11) only the most singular scattering processes by putting $i\omega_{n+} \rightarrow E_{L'}(\mathbf{k}_+)/\hbar$ and $i\omega_n \rightarrow E_L(\mathbf{k})/\hbar$, in two single-particle self-energies, $\Sigma_L(\mathbf{k}, i\omega_n)$ and $\Sigma_{L'}(\mathbf{k}_+, i\omega_{n+})$, and in the related vertex corrections on the right-hand side of the equations. In this way, the expression in the brackets on the left-hand side does not depend on $i\omega_n$, and the equations can be rewritten in terms of the intraband ($L = L'$) and interband ($L \neq L'$) induced densities $\delta n^{LL'}(\mathbf{k}, \omega)$ defined by

$$\begin{aligned} \delta n^{LL'}(\mathbf{k}, \omega) = \sum_{\mathbf{k}'} \frac{1}{\hbar} \mathcal{D}^{LL'}(\mathbf{k}, \mathbf{k}_+, \mathbf{k}'_+, \mathbf{k}', \omega) \\ \times e q^{L'L}(\mathbf{k}_+, \mathbf{k}) V^{\text{ext}}(\mathbf{q}, \omega). \end{aligned} \quad (12)$$

Here

$$e q^{L'L}(\mathbf{k}_+, \mathbf{k}) V^{\text{ext}}(\mathbf{q}, \omega) \equiv \frac{\hbar J_\alpha^{L'L}(\mathbf{k})}{E_{L'L}(\mathbf{k}_+, \mathbf{k})} iE_\alpha(\omega), \quad (13)$$

with $E_\alpha(\omega)$ and $V^{\text{ext}}(\mathbf{q}, \omega) = (i/q_\alpha)E_\alpha(\omega)$ being, respectively, the external electric field and the related scalar potential (notice that for $L = L'$ Eq. (13) reduces to the expression $eV^{\text{ext}}(\mathbf{q}, \omega) = e(i/q_\alpha)E_\alpha(\omega)$ that is independent of \mathbf{k}). Furthermore, $q^{L'L}(\mathbf{k}_+, \mathbf{k})$ is the charge vertex, given by Eqs. (A8) and (29), $J_\alpha^{L'L}(\mathbf{k})$ is the current vertex and $\mathbf{q} = q_\alpha \hat{e}_\alpha$.

In Eq. (12), $\mathcal{D}^{LL'}(\mathbf{k}, \mathbf{k}_+, \mathbf{k}'_+, \mathbf{k}', \omega)$ is obtained by the analytical continuation of $\mathcal{D}^{LL'}(\mathbf{k}, \mathbf{k}_+, \mathbf{k}'_+, \mathbf{k}', i\nu_n)$, $i\nu_n \rightarrow \omega + i\eta$. The summation of Eqs. (11) over $i\omega_n$ makes the single-particle self-energy contributions and the related vertex corrections to appear on the same footing, resulting in the electron-hole self-energy of the form

$$\begin{aligned} \hbar \Pi_\alpha^{LL'}(\mathbf{k}, \omega) \\ \approx - \sum_{\lambda\mathbf{q}'} \sum_{s=\pm 1, -1} \frac{|G_\lambda(\mathbf{q}')|^2}{N} \left\{ 1 - \frac{\tilde{J}_\alpha^{LL'}(\mathbf{k} + \mathbf{q}')}{\tilde{J}_\alpha^{LL'}(\mathbf{k})} \right\} \\ \times \left[\frac{f_\lambda^b(\mathbf{q}') + f(sE_{L'}(\mathbf{k} + \mathbf{q}'))}{\hbar\omega + i\eta + E_{LL'}(\mathbf{k}, \mathbf{k} + \mathbf{q}') + s\hbar\omega_{\lambda\mathbf{q}'}} \right. \\ \left. + \frac{f_\lambda^b(\mathbf{q}') + f(sE_L(\mathbf{k} + \mathbf{q}'))}{\hbar\omega + i\eta + E_{LL'}(\mathbf{k} + \mathbf{q}', \mathbf{k}) - s\hbar\omega_{\lambda\mathbf{q}'}} \right]. \end{aligned} \quad (14)$$

The corresponding generalization of $\Pi_\alpha^{LL'}(\mathbf{k}, \omega)$ to the case with the interband electron-phonon coupling is straightforward; however, it is beyond the scope of the present work. $f_\lambda^b(\mathbf{q}')$ and $f(E_L(\mathbf{k})) \equiv f_L(\mathbf{k})$ in Eq. (14) are, respectively, the Bose–Einstein and Fermi–Dirac distribution functions. Finally, notice that the electron scattering on the static disorder, described by the potential $V_1(\mathbf{q}')$, is included here through the replacement $\omega_{\lambda\mathbf{q}'} \rightarrow 0$ and $(1 + 2f_\lambda^b(\mathbf{q}'))|G_\lambda(\mathbf{q}')|^2/N \rightarrow |V_1(\mathbf{q}')|^2$ in the $\lambda = 0$ boson branch [20].

C. Transport equations and optical conductivity

The resulting self-consistent equation for the densities $\delta n^{LL'}(\mathbf{k}, \omega)$ represents the generalization of the transport equation [20, 22],

$$[\hbar\omega + E_{LL'}(\mathbf{k}, \mathbf{k}_+)]\delta n^{LL'}(\mathbf{k}, \omega) + \hbar\Pi_\alpha^{LL'}(\mathbf{k}, \omega)\delta\tilde{n}^{LL'}(\mathbf{k}, \omega) = \frac{f_L(\mathbf{k}) - f_{L'}(\mathbf{k}_+)}{E_{L'L}(\mathbf{k}_+, \mathbf{k})} i\hbar J_\alpha^{L'L}(\mathbf{k})E_\alpha(\omega). \quad (15)$$

In this equation $\delta\tilde{n}^{LL'}(\mathbf{k}, \omega)$ is the contribution to $\delta n^{LL'}(\mathbf{k}, \omega)$ proportional to $\tilde{J}_\alpha^{L'L}(\mathbf{k})$ (the effective current vertices in Eqs. (14) and (15) are $\tilde{J}_\alpha^{LL}(\mathbf{k}) = J_\alpha^{LL}(\mathbf{k})$ in the intraband channel and $\tilde{J}_\alpha^{L'L}(\mathbf{k}) = \hbar\omega J_\alpha^{L'L}(\mathbf{k})/E_{L'L}(\mathbf{k}, \mathbf{k})$ in the interband channel). Equation (15) is solved consistently with the charge continuity equation and combined with the definition of the optical conductivity tensor. The result is the optical conductivity of the effective single-particle multiband models [19, 20, 21, 25]

$$\sigma_{\alpha\alpha}^{\text{sp}}(\omega) = \frac{i}{\omega} \frac{1}{V} \sum_{LL'\mathbf{k}\sigma} \left(\frac{\hbar\omega}{E_{L'L}(\mathbf{k}_+, \mathbf{k})} \right)^{n_{LL'}} |J_\alpha^{LL'}(\mathbf{k})|^2 \quad (16)$$

$$\times \frac{f_L(\mathbf{k}) - f_{L'}(\mathbf{k}_+)}{\hbar\omega + \hbar\Pi_\alpha^{LL'}(\mathbf{k}, \omega) + E_{LL'}(\mathbf{k}, \mathbf{k}) - \frac{E_{L'L}^2(\mathbf{k}, \mathbf{k}_+)}{\hbar\omega}},$$

with $n_{LL} = 1$ in the intraband channel and $n_{L'L} = 2$ in the interband channel. In the dynamical limit, the last term in the denominator can be safely neglected. At this point it should be recalled that the current vertices $J_\alpha^{LL'}(\mathbf{k})$ can be shown in simple physical terms as: $J_\alpha^{LL}(\mathbf{k}) = ev_\alpha^L(\mathbf{k})$ in the intraband channel and $J_\alpha^{L'L}(\mathbf{k}) = (i/\hbar)P_\alpha^{L'L}(\mathbf{k})E_{L'L}(\mathbf{k}, \mathbf{k})$ in the interband channel; $v_\alpha^L(\mathbf{k})$ is the electron group velocity and $P_\alpha^{L'L}(\mathbf{k})$ is the related interband dipole vertex. It should also be noticed that the coherence factor in the textbook expression for the interband contributions [5, 8] is slightly different from that in Eq. (16), as well as that the phenomenological extension of the textbook expression is found to lead to the non-physical in-gap spectra (see Fig. 1 in Ref. [17]).

D. $\Delta = 0$ case

Before turning to the detailed numerical analysis of the expression (16), let us write Eqs. (15) and (16) ex-

plicitly for the (single-band) case in which $\Delta = 0$ and the relaxation rate Γ is presumably small but finite ($\text{Im}\{II_\alpha^0(\mathbf{k}, \omega)\} \approx \Gamma$). These expressions will make the comparison of the present approach with the common CDW approaches in Sec. 5 straightforward.

For $\Delta = 0$ and $\mathbf{q} = q_x \hat{e}_x$, the electron-hole-pair energy is $\varepsilon(\mathbf{k}_+) - \varepsilon(\mathbf{k}) \approx \hbar\omega_0(\mathbf{q}) = \hbar q_x v_x^0(\mathbf{k})$, with $\omega_0^2(\mathbf{q})$ being independent of \mathbf{k} for $\mathbf{k} \approx \mathbf{k}_F$. Eq. (15) can be written now in the textbook form [22]

$$\begin{aligned} \omega\delta n_0(\mathbf{k}, \omega) - \omega_0(\mathbf{q})\delta n_1(\mathbf{k}, \omega) &= 0, \\ (\omega + i\Gamma)\delta n_1(\mathbf{k}, \omega) - \omega_0(\mathbf{q})\delta n_0(\mathbf{k}, \omega) &= (-) \frac{\partial f(\mathbf{k})}{\partial \varepsilon(\mathbf{k})} iev_x^0(\mathbf{k})E_x(\omega). \end{aligned} \quad (17)$$

Introducing the boson field $\psi(\mathbf{q}, \omega)$, which time derivative is proportional to the current induced by the external electric field,

$$j_x^{\text{ind}}(\omega) = \frac{1}{V} \sum_{\mathbf{k}\sigma} ev_x^0(\mathbf{k})\delta n_1(\mathbf{k}, \omega) \equiv \frac{e}{\pi} \dot{\psi}(\mathbf{q}, \omega), \quad (18)$$

one obtains the equation of motion

$$m[\omega(\omega + i\Gamma) - \omega_0^2(\mathbf{q})]\psi(\mathbf{q}, \omega) = e\pi n_{xx}^{\text{eff},0} E_x(\omega). \quad (19)$$

The resulting optical conductivity is given by the interband term in Eq. (16), i.e., by the expressions

$$\begin{aligned} \sigma_{xx}(\omega) &= \frac{e^2 n_{xx}^{\text{eff},0}}{m} \frac{i\omega}{\omega(\omega + i\Gamma) - \omega_0^2(\mathbf{q})} \\ &\equiv \frac{i\omega}{\hbar} \left(\frac{e}{\pi} \right)^2 V \mathcal{D}_\psi^0(\mathbf{q}, \omega). \end{aligned} \quad (20)$$

Here $\mathcal{D}_\psi^0(\mathbf{q}, \omega)$ is the bare propagator of the field $\psi(\mathbf{q}, \omega)$, $n_{xx}^{\text{eff},0}$ is the effective number of conduction electrons,

$$n_{xx}^{\text{eff},0} = -\frac{m}{V} \sum_{\mathbf{k}\sigma} (v_x^0(\mathbf{k}))^2 \frac{\partial f(\mathbf{k})}{\partial \varepsilon(\mathbf{k})} = \frac{2}{\pi} \frac{m_{aa} v_x^0(k_F)}{\hbar}, \quad (21)$$

$v_x^0(\mathbf{k}) = (1/\hbar)\partial\varepsilon(\mathbf{k})/\partial k_x$ is the bare electron group velocity and $m_{aa} = 2\hbar^2/(t_a a^2)$ is the mass parameter.

IV. DISCUSSION

A. Underdamped regime

For comparison with the textbook expressions for the single-particle contributions to the optical conductivity, it is convenient to turn back to the simplest case discussed in Sec. 3.1. The electron-hole self-energy is approximated by its imaginary part and the imaginary part is assumed to be small when compared to the interband threshold energy; i.e., $\Pi_\alpha^{LL'}(\mathbf{k}, \omega) \approx i\Pi_\alpha^{LL'}(\mathbf{k}, \omega)$ and $\Gamma_\alpha^{LL'}(\mathbf{k}, \omega) \approx \Gamma_\alpha^{LL'}$ ($\Gamma_\alpha^{LL} \equiv \Gamma_\alpha^{\text{intra}}$ and $\Gamma_\alpha^{L'L} \equiv \Gamma_\alpha^{\text{inter}}$, hereafter). In the underdamped regime ($\Gamma_\alpha^{\text{inter}} \ll 2\Delta$), this approximation

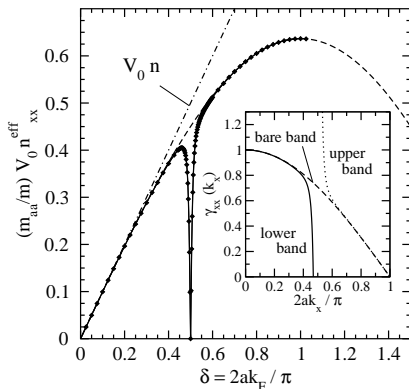


FIG. 4: Main figure: The normalized effective number of conduction electrons $(m_{aa}/m)V_0 n_{xx}^{\text{eff}}$ as a function of the band filling for $2t_a = 0.5$ eV, $2t_b = 0$, $T \rightarrow 0$ and $\Delta_0 = 0$ (dashed line) and 10 meV (solid line). The diamonds represent the dimensionless electron group velocity $[2/(t_a \pi^2)]v_x^0(k_F)$. Inset: The inverse effective mass tensors $\gamma_{xx}^{CC}(\mathbf{k})$ for $Q_x = 0.5\pi/a$ and $\Delta_0 = 10$ meV (solid and dotted lines, respectively). The bare-band vertex ($\Delta = 0$, dashed line) is given for comparison.

does not affect the spectrum in a critical manner, neither in the metallic regime (with $2k_F$ not too close to Q_x), nor in the CDW state at temperatures well below the critical temperature. In the metallic case, the effective numbers of conduction electrons in the resistivity, or in the Drude part of the optical conductivity, consist of two parts, the residual one, which remains finite at $T \rightarrow 0$, and the thermally activated part. In the $t_b \rightarrow 0$ Peierls case there are only thermally activated electrons. Finally, in the Peierls case with t_b/Δ not too small there is a portion of the Fermi surface on which the CDW gap is not developed, leading again to a finite residual number of conduction electrons.

To compare briefly the correct estimations of these numbers with the oversimplified “semiconducting” expressions encountered in the literature [26], we apply Eq. (16) now to the simplest metallic situation corresponding to $\mathbf{Q} = (0.5\pi/a, 0)$ and $t_b \rightarrow 0$. In this respect, it should be noticed that the present analysis is not focussed on the single-particle properties of the usual strictly 1D model, the physics of which is dominated by the singular nature of the forward scattering processes in the single-electron self-energy. Instead, we consider the electron-hole excitations in the typical Q1D model in which the Q1D character is incorporated in the aforementioned form of the electron-hole self-energy, where the forward scattering contributions are removed by the Ward identity cancellation of the $\mathbf{q} \approx 0$ self-energy and vertex corrections in Eq. (14). The $t_b \rightarrow 0$ limit serves here only to replace most of the integrations over the 2D Brillouin zone by the 1D integrations. The results obtained in this way can be compared term by term to the well-known analytical expressions.

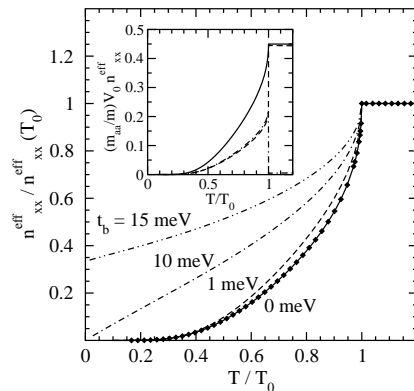


FIG. 5: Main figure: The temperature dependence of the normalized effective number of conduction electrons in the (imperfectly nested $Q_y = 0$) CDW state for $2t_a = 0.5$ eV, $2t_b = 0$ (solid line), 1 meV (dashed line), 10 meV (dot-dashed line) and 15 meV (dot-dot-dashed line), $2k_F = Q_x = 0.5\pi/a$, $T_0 = 66.7$ K and $\Delta_0 = 10$ meV. The diamonds represent the function $\exp\{-\Delta(T)/(k_B T)\}$.

For example, the intraband conductivity along the highly conducting direction is proportional to the effective number of conduction electrons n_{xx}^{eff} , as seen from

$$\sigma_{\alpha\alpha}^{\text{intra}}(\omega) \approx \frac{ie^2 n_{\alpha\alpha}^{\text{eff}}}{m(\omega + i\Gamma_{\alpha}^{\text{intra}})}, \quad (22)$$

for $\alpha = x$. $n_{\alpha\alpha}^{\text{eff}}$ includes the contributions of both bands, and it can be shown in two alternative ways, as a surface integral in the \mathbf{k} space, or the related volume integral,

$$\begin{aligned} n_{\alpha\alpha}^{\text{eff}} &= \sum_L n_{\alpha\alpha}^{\text{eff}}(L) = -\frac{m}{V} \sum_{Lk\sigma} (v_{\alpha}^L(\mathbf{k}))^2 \frac{\partial f_L(\mathbf{k})}{\partial E_L(\mathbf{k})} \\ &= \frac{1}{V} \sum_{Lk\sigma} \gamma_{\alpha\alpha}^{LL}(\mathbf{k}) f_L(\mathbf{k}). \end{aligned} \quad (23)$$

In the first representation, it is given in terms of the electron group velocity, while in the second representation it depends on the dimensionless inverse effective-mass tensor $\gamma_{\alpha\alpha}^{LL}(\mathbf{k}) = (m/\hbar)\partial v_{\alpha}^L(\mathbf{k})/\partial k_{\alpha}$. The dependence of n_{xx}^{eff} on the electron doping $\delta = 2ak_F/\pi$ is shown in Fig. 4 for two choices of the distortion potential, $\Delta_0 = 0$ and 10 meV, and $T \rightarrow 0$. The electron doping $\delta = nV_0$ (n is the concentration of electrons and V_0 is the primitive cell volume of the $\Delta_0 = 0$ lattice) and the dimensionless electron group velocity are also given for comparison. The latter represents the analytical solution of the $t_b \rightarrow 0$ model.

The metallic regime of the primary experimental interest corresponds to the case of a low electron/hole doping with respect to the quarter-filled band. In this case, the residual part in n_{xx}^{eff} (shown in Fig. 4) is small when compared to its $\Delta = 0$ value (dashed line in the figure). Even for relatively low temperatures, the thermally activated part in n_{xx}^{eff} becomes important, leading to pronounced thermal effects in n_{xx}^{eff} . The thermal effects in the Drude part of the optical conductivity, or in

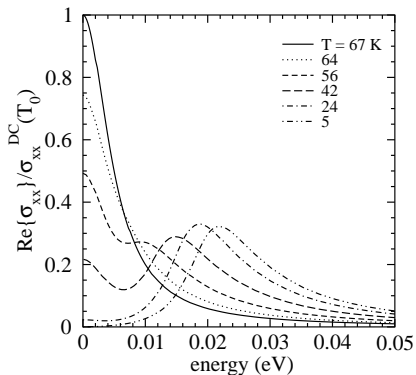


FIG. 6: The development of the normalized total optical conductivity with temperature in the underdamped regime: $2t_a = 0.5$ eV, $2t_b = 1$ meV, $T_0 = 66.7$ K, $\Delta_0 = 10$ meV and $\hbar\Gamma_a^{\text{intra}} = \hbar\Gamma_a^{\text{inter}} = 5$ meV.

the resistivity, are further illustrated in Fig. 5 for the imperfectly nested CDW case (corresponding to the electron doping $\delta = 0.5$ in Fig. 4). The temperature dependence of the activation energy Δ is parametrized as $\Delta(T) = \Delta_0(1 - T/T_0)^\beta$, with $\beta = 1/2$. n_{xx}^{eff} is shown for four different values of t_b and compared to the empirical expression $n_{xx}^{\text{eff}}(T) = \exp\{-\Delta(T)/(k_B T)\} n_{xx}^{\text{eff}}(T_0)$ (the residual part in n_{xx}^{eff} corresponds to the zero-temperature interception value). The dashed and dot-dashed lines in the inset of figure represent the partial contributions of the lower and upper band for $t_b = 0$, $n_{xx}^{\text{eff}}(\underline{C})$ and $n_{xx}^{\text{eff}}(\underline{C})$ in Eq. (23), respectively. The latter two have to be contrasted to the numbers

$$n_h = \frac{1}{V} \sum_{\mathbf{k}\sigma} [1 - f_C(\mathbf{k})], \quad n_e = \frac{1}{V} \sum_{\mathbf{k}\sigma} f_{\underline{C}}(\mathbf{k}) \quad (24)$$

invoked from the theory of the ordinary semiconductors. The numbers (24) are often taken as a good approximation for $n_{xx}^{\text{eff}}(\underline{C})$ and $n_{xx}^{\text{eff}}(\underline{C})$. However, the disagreement between the expressions (24) and experimental observation is typically of two orders of magnitude [27], and, consequently, the analyses based on the numbers (24) have to be taken with reservation. For the parameters used in Fig. 5, we obtain a factor of 25. This disagreement is easily understood on noting that the semiconducting approach, Eq. (24), completely neglects the coherence effects in the inverse effective-mass tensor. In other words, by replacing the vertices $\gamma_{xx}^{LL}(\mathbf{k})$ by unity, when the numbers $n_{xx}^{\text{eff}}(\underline{C})$ and $n_{xx}^{\text{eff}}(\underline{C})$ reduce to n_h and n_e indeed, this approach does not take carefully into account the fact that the thermally activated electrons are related only to the states in the thermal window around the Fermi level. Notice in this respect the singular behavior of the vertices $\gamma_{xx}^{LL}(\mathbf{k})$ at $2k_x = 0.5\pi/a$, shown in the inset of Fig. 4, which dominates the behavior of n_{xx}^{eff} for $2k_F \approx 0.5\pi/a$. On the contrary, the common approaches based on the surface-integral representation of $n_{\alpha\alpha}^{\text{eff}}$ usually give rise to the correct results.

Another important observation is that the optical conductivity model (16) has a quite general form and is thus applicable to variety of low-dimensional systems. In this respect one should notice that the values of the effective numbers $n_{\alpha\alpha}^{\text{eff}}$ are generally a direct consequence of the coherent scattering of conduction electrons on the crystal potential or on the periodically distorted lattice, irrespective of the band filling. These numbers represent the numbers of effectively free charge carriers, with the thermally activated part being usually very sensitive to temperature, providing the estimation of the activation energy Δ , or the charge-transfer gap in the general case. The corresponding numbers of bound charges, on the other hand, are the numbers of excited electrons across the CDW gap [8] or across the charge-transfer gap. The latter numbers depend on temperature as well, as seen from the interband part of Eq. (16), which can be rewritten in the form

$$\sigma_{\alpha\alpha}^{\text{inter}}(\omega) \approx i\omega \frac{1}{V} \sum_{L \neq L', \mathbf{k}\sigma} |P_{\alpha}^{LL'}(\mathbf{k})|^2 \times \frac{f_L(\mathbf{k}) - f_{L'}(\mathbf{k})}{\hbar\omega + i\hbar\Gamma_{\alpha}^{\text{inter}} + E_{LL'}(\mathbf{k}, \mathbf{k})}. \quad (25)$$

The temperature dependence of the total optical conductivity $\sigma_{xx}^{\text{SD}}(\omega) = \sigma_{xx}^{\text{intra}}(\omega) + \sigma_{xx}^{\text{inter}}(\omega)$ is calculated for several underdamped regimes. The damping energies $\hbar\Gamma_a^{\text{intra}}$ and $\hbar\Gamma_a^{\text{inter}}$ are assumed to be temperature independent, for simplicity, and small in comparison with the scale 2Δ . The results for the imperfectly nested case are shown in Fig. 6 and are essentially the same as the results of the analogous nearly half-filled dimerized band [19, 25]. Although it is physically clear that at temperatures T well below T_c Γ_a^{inter} is much larger than Γ_a^{intra} , the spectra shown in Fig. 6 are calculated for $\Gamma_a^{\text{intra}} = \Gamma_a^{\text{inter}}$, for clarity. The shift of the MIR maximum in the spectra ($\hbar\omega_{\text{MIR}}$) with temperature follows roughly the energy scale 2Δ , giving an alternative method of estimating Δ [5]. The spectra are also characterized by the in-gap optical excitations, mainly in the energy range from $\hbar\omega_{\text{min}} \approx 2\Delta - \hbar\Gamma_a^{\text{inter}}$ to 2Δ . The cut-off energy $\hbar\omega_{\text{min}}$ is associated with the zero conductivity interception of the line obtained by the linear extrapolation of the interband conductivity. The square-root singularity at $\hbar\omega = 2\Delta$ is absent here, and, according to Ref. [18], the same shape of $\sigma_{xx}^{\text{inter}}(\omega)$ is expected down to zero temperature.

B. Overdamped regime

A completely different situation appears in the overdamped regime where the damping energy $\hbar\Gamma_a^{\text{inter}}$ becomes comparable to 2Δ and where the real part of the electron-hole self-energy starts playing an important role. Typical physical situation corresponding to this regime is the CDW instability of the magnetic metals, where the wide band electrons exhibit the CDW instability, and are usually scattered by the strongly correlated electrons in

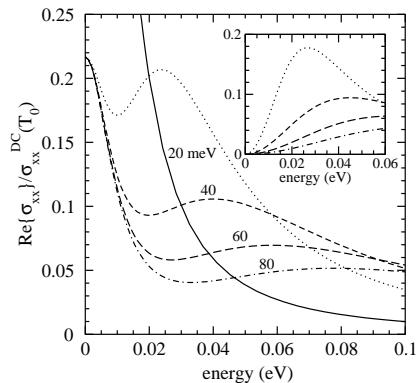


FIG. 7: Main figure: The optical conductivity as a function of damping energy $\hbar\Gamma_a^{\text{inter}}$ at $T = 42$ K. Dotted, dashed, long-dashed and dot-dashed lines correspond to $\hbar\Gamma_a^{\text{inter}} = 20, 40, 60$ and 80 meV, respectively. The other parameters are the same as in Fig. 6. The solid line in the total optical conductivity at $T = 67$ K. Inset: The related interband contributions (the parameters are the same as in the main figure).

one or more narrow bands. As the present discussion of the general expression (16) neglects the real part of the self-energy, it turns out to be inappropriate for the detailed quantitative analysis of the overdamped regime, but it satisfactorily explains the interplay between two mutually competing energy scales, $\hbar\Gamma_a^{\text{inter}}$ and 2Δ . Fig. 7 shows typical results. The position of the MIR peak is at $\hbar\omega_{\text{MIR}} \approx \sqrt{4\Delta^2 + (\hbar\Gamma_a^{\text{inter}})^2}$. In this case, $\hbar\omega_{\text{min}}$ is a rather complicated function of the model parameters, but it is close to the value obtained in the narrow band limit of $\sigma_{xx}^{\text{inter}}(\omega)$, where all interband excitations are assumed to appear close to the threshold energy $E_{\underline{C}\underline{C}}(\mathbf{k}, \mathbf{k}) \approx 2\Delta$. In this case, one obtains

$$\text{Re}\{\sigma_{xx}^{\text{inter}}(\omega)\} \propto \frac{\hbar\omega\hbar\Gamma_a^{\text{inter}}}{(\hbar\omega - 2\Delta)^2 + (\hbar\Gamma_a^{\text{inter}})^2} \times \frac{8\hbar\omega\Delta}{(\hbar\omega + 2\Delta)^2 + (\hbar\Gamma_a^{\text{inter}})^2}. \quad (26)$$

As a result, in the overdamped regime $\hbar\omega_{\text{min}}$ increases with increasing $\hbar\Gamma_a^{\text{inter}}$, for example, from the value $\hbar\omega_{\text{min}} \approx \Delta$ at $\hbar\Gamma_a^{\text{inter}} = 5\Delta$ to $\hbar\omega_{\text{min}} \approx 2\Delta$ at $\hbar\Gamma_a^{\text{inter}} = 10\Delta$. Knowing the experimental values of $\hbar\omega_{\text{MIR}}$ and $\hbar\omega_{\text{min}}$, we can again estimate Δ and $\hbar\Gamma_a^{\text{inter}}$ and compare Δ to the activation energy of transport coefficients.

As mentioned in the introduction, a clear evidence of the overdamped regime is recently found in the vanadium chain compound BaVS_3 [3]. BaVS_3 is the multiband system with the (commensurate) CDW instability in which one weakly correlated wide band and two strongly correlated narrow bands coexist at the Fermi level. Thanks to the extensive experimental activity in this system in recent years [1, 2, 3, 4], BaVS_3 seems to be a good candidate for detailed investigation of the overdamped regime.

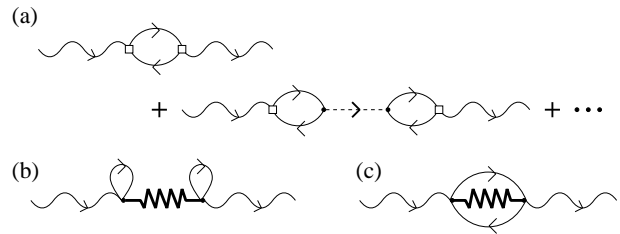


FIG. 8: (a) The collective contribution to the optical conductivity in the common 1D models with the forward-scattering short-range interactions. (b) The collective contribution in the present model. (c) The Hopfield-like processes neglected in the present approach.

V. COMPARISON WITH THE COMMON CDW THEORIES

In the low-energy examinations of the CDW systems it is common to use different strictly 1D models with the non-retarded short-range interactions in which not only the forward-scattering but also the backward-scattering processes in the electron-hole self energy are neglected [15, 16]. These approaches are usually based on the bosonization procedure. For example, for the simplest case with only the forward-scattering interaction g_4 taken into account, the optical conductivity is given by the RPA diagrams in Fig. 8(a). The first diagram is nothing but the ideal intraband conductivity of Eq. (20). The interaction g_4 leads to the renormalization of the electron group velocity in Eqs. (20) and (21) in the way that

$$v_x^0(\mathbf{k}) \rightarrow u_\rho = \sqrt{\frac{m}{m^*}} v_x^0(k_F),$$

while the electron dispersions in $\partial f(\mathbf{k})/\partial \varepsilon(\mathbf{k})$, together with the related density of states, remain unaffected by g_4 . The boson field $\psi(\mathbf{q}, \omega)$ is found to satisfy the equation of motion (19), while the optical conductivity is found to be given by Eqs. (20), (21), with $v_x^0(\mathbf{k}) \rightarrow u_\rho$ [9, 16].

The present Q1D model differs from these strictly 1D models in three important points. First, the electron-electron interactions in question are the retarded, phonon-mediated interactions [5, 6, 7], second, the collective infrared-active mode is the phase phonon mode, which participates in the total conductivity spectral weight with usually less than 0.5 % (e.g., m^* is of the order of $400m$ in $\text{K}_{0.3}\text{MoO}_3$ [28]), and, finally, the external electric fields are assumed to be well below the critical field required to give the non-linear conductivity [12, 13].

In this section, we want to determine the structure of the photon-phase phonon coupling, and to compare the obtained results with both the textbook results obtained within the same Q1D model [5, 6, 7, 8] and the results of strictly 1D models [9, 16]. We will derive here, for the first time, a clear selection rule for the infrared-active

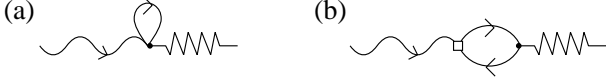


FIG. 9: (a) The direct photon-phonon coupling and (b) the indirect, electron-mediated photon-phonon coupling in pure CDW systems.

(and Raman-active) phonon modes. On the qualitative level, the arguments are the following. For the quarter-filled case shown in Fig. 1, the electric fields couple to the dipole moment of the phase phonon mode (the dipole moment is carried by the bound (condensed) electrons). For Δ comparable to the band width, this mode is the ordinary infrared-active phonon mode, characterized by the effective ion charge $q = q_c/\sqrt{2}$, the reduced ion mass M and the concentration of ions $1/V_0$. On the other hand, for Δ small in comparison with the band width, the electrons in question are only weakly bound and the magnitude of the dipole is now proportional to \tilde{e} , which is q multiplied by the ratio between the amplitudes of the electron and ion oscillations. In the limit $\Delta \rightarrow 0$, the dipole moment vanishes.

To discuss this question quantitatively, we neglect again the Umklapp processes in the electron dispersions and focus the attention on the $\alpha = 0$ two-band model of Eq. (4). In this case, all relevant vertex functions are simple functions of the auxiliary phase $\varphi(\mathbf{k})$ defined by

$$\tan \varphi(\mathbf{k}) = \frac{2\Delta}{\varepsilon_{cc}(\mathbf{k})}. \quad (27)$$

In the long wavelength limit, the electron-phonon vertices and the charge vertices of Eqs. (A5) and (A8) become

$$\begin{aligned} g_A^{CC}(\mathbf{k}_+, \mathbf{k}) &= -g_A^{CC}(\mathbf{k}_+, \mathbf{k}) \\ &= -\sin \frac{\varphi(\mathbf{k}_+) + \varphi(\mathbf{k})}{2} \approx -\sin \varphi(\mathbf{k}), \\ g_A^{CC}(\mathbf{k}_+, \mathbf{k}) &\approx e^{i\phi(\mathbf{k})} \cos \varphi(\mathbf{k}), \\ g_\varphi^{CC}(\mathbf{k}_+, \mathbf{k}) &= g_\varphi^{CC}(\mathbf{k}_+, \mathbf{k}) \\ &= i \sin \frac{\varphi(\mathbf{k}) - \varphi(\mathbf{k}_+)}{2} \approx \mathcal{O}(q_\alpha), \\ g_\varphi^{CC}(\mathbf{k}_+, \mathbf{k}) &\approx ie^{i\phi(\mathbf{k})}, \end{aligned} \quad (28)$$

$$\begin{aligned} q^{CC}(\mathbf{k}_+, \mathbf{k}) &\approx q^{CC}(\mathbf{k}_+, \mathbf{k}) \approx 1, \\ q^{CC}(\mathbf{k}_+, \mathbf{k}) &\approx \frac{\hbar}{e} \frac{q_\alpha J_\alpha^{CC}(\mathbf{k})}{E_{CC}(\mathbf{k}_+, \mathbf{k})}. \end{aligned} \quad (29)$$

According to Fig. 9, the photon-phonon coupling consists of two contributions, the direct coupling and the indirect, electron-mediated coupling. In the commensurate case in which the Hopfield-like processes [29] of Fig. 8(c) are neglected, the linear direct coupling between external electromagnetic fields ($E_x(-\mathbf{q})$ is the electric component of the field polarized along the highly conducting direction) and two $\mathbf{q} \approx 0$ phonon modes under consideration

(Fig. 9(a)) is given by the ground-state average of the coupling Hamiltonian

$$\begin{aligned} H_1^{\text{ext}} &= -\sum_{\lambda\mathbf{q}} E_x(-\mathbf{q}) \sum_{LL'\mathbf{k}\sigma} \delta P_{x\lambda}^{L'L}(\mathbf{k}, \mathbf{q}) c_{L'\mathbf{k}\sigma}^\dagger c_{L\mathbf{k}\sigma} \\ \delta P_{x\lambda}^{L'L}(\mathbf{k}, \mathbf{q}) &= \frac{s_\lambda e}{\sqrt{2N}} g_\lambda^{L'L}(\mathbf{k}, \mathbf{k}) \tilde{u}_{x\lambda\mathbf{q}} \end{aligned} \quad (30)$$

($s_A = -1$, $s_\varphi = 1$ and the indices in the vertex $g_\lambda^{L'L}(\mathbf{k}, \mathbf{k})$ are $\underline{A} = \varphi$, $\underline{\varphi} = A$). Here $\tilde{u}_{x\lambda\mathbf{q}}$ is the amplitude of the electron oscillations and $\delta P_{x\lambda}^{L'L}(\mathbf{k}, \mathbf{q})$ is the related dipole vertex. For the incommensurate case, the direct coupling is given in a similar way in terms of the current vertex

$$\delta J_{x\lambda}^{L'L}(\mathbf{k}, \mathbf{q}) = \frac{s_\lambda e}{\sqrt{2N}} g_\lambda^{L'L}(\mathbf{k}, \mathbf{k}) \frac{\partial}{\partial t} \tilde{u}_{x\lambda\mathbf{q}}. \quad (31)$$

Since the phase phonon field can be written as $u_{x\varphi\mathbf{q}} = 2i\langle u_A \rangle \varphi_{\mathbf{q}}$ [5], we obtain again that the current vertex is proportional to the time derivative $\dot{\varphi}_{\mathbf{q}}$, and the related equation of motion is analogous to Eq. (19), with e , m , $n_{xx}^{\text{eff},0}$ and $\omega_0(\mathbf{q})$ replaced by \tilde{e} , M , $1/V_0$ and $\omega_{\varphi\mathbf{q}}$. These parameters enter into the optical conductivity expression through two adjustable parameters (m^* and $\omega_{\varphi\mathbf{q}}$ in Eq. (6), for example).

As a result, the direct photon-phonon coupling constant amounts to the replacement of $c_{L'\mathbf{k}\sigma}^\dagger c_{L\mathbf{k}\sigma}$ in Eq. (30) by $\langle c_{L'\mathbf{k}\sigma}^\dagger c_{L\mathbf{k}\sigma} \rangle = \delta_{L,C} \delta_{L',C} f_C(\mathbf{k})$. This result shows that the coupling function of the (Raman-active) mode $u_{A\mathbf{q}}$, $g_\varphi^{CC}(\mathbf{k}, \mathbf{k})$, vanishes, while the coupling function of the phase phonon mode $u_{\varphi\mathbf{q}}$ is finite and, as mentioned above, is proportional to the magnitude of the charge-density wave q_c , which is given by

$$q_c = -e \frac{1}{N} \sum_{\mathbf{k}\sigma} \sin \varphi(\mathbf{k}) f_C(\mathbf{k}). \quad (32)$$

Notice that the fact that the phonons $\mathbf{u}_{\lambda\mathbf{q}}$ in Eq. (30) couple to external electromagnetic fields through the function $g_\lambda^{CC}(\mathbf{k}, \mathbf{k})$, rather than $g_\lambda^{AA}(\mathbf{k}, \mathbf{k})$, is a consequence of the fact that the variations $V_\lambda(\mathbf{r}_i)$ in Eq. (2) are proportional to the derivative of $\mathbf{u}_{\lambda i}$ with respect to \mathbf{r}_i , rather than to the displacement vector $\mathbf{u}_{\lambda i}$.

In the Hopfield-like processes the photon momentum is shared between an electron-hole pair and a infrared-active phonon in the way described by the dipole density operator

$$\sum_{LL'\mathbf{q}'\mathbf{k}\sigma} \delta P_{x\varphi}^{L'L}(\mathbf{k} + \mathbf{q}' - \mathbf{q}, \mathbf{k}, \mathbf{q}') c_{L'\mathbf{k}+\mathbf{q}'-\mathbf{q}\sigma}^\dagger c_{L\mathbf{k}\sigma}$$

in Eq. (30), with $g_A^{L'L}(\mathbf{k}, \mathbf{k})$ in the dipole vertex replaced by $g_A^{L'L}(\mathbf{k} + \mathbf{q}' - \mathbf{q}, \mathbf{k})$. The sum over states in the phase phonon branch (\mathbf{q}') is restricted to the region where the vertex $g_A^{L'L}(\mathbf{k} + \mathbf{q}' - \mathbf{q}, \mathbf{k})$ of Eq. (A5) is non-zero.

The indirect, electron-mediated photon-phonon coupling shown in Fig. 9(b), on the other hand, is given by the interband correlation function $\chi_{1,\lambda}^{\text{inter}}(\mathbf{q}, \omega)$ defined

in Appendix, or by Eq. (4.3) in Ref. [7]. According to Eqs. (28) and (29), the product of vertices $q^{\underline{C}C}(\mathbf{k}, \mathbf{k}_+)$ and $g_\lambda^{\underline{C}C}(\mathbf{k}_+, \mathbf{k})$ in this correlation function is proportional to $\exp\{-\phi(\mathbf{k})\}J_x^{\underline{C}C}(\mathbf{k})$, i.e., it is proportional to the bare electron group velocity $v_x^0(\mathbf{k})$. $v_x^0(\mathbf{k})$ is an odd function of k_x and, consequently, the coupling function $\chi_{1,\lambda}^{\text{inter}}(\mathbf{q}, \omega)$ vanishes for both phonon branches. The background of this result is the fact that the electron-phonon coupling g is independent of the electron wave vectors. A more complicated form of the infrared selection rules and the photon-phase phonon coupling functions can be expected in the models in which the electron-phonon coupling is related to the variations of the bond energies [6] (namely, g depends now on the electron wave vectors, introducing a new channel in the electron-photon coupling).

Finally, it is important to notice that the common textbook analyses [5, 7, 8] explain the photon-phase phonon coupling in the way (see Eqs. (4.3) and (4.7) in Ref. [7]) which is formally equivalent to the replacement of the bare electron group velocity in $\chi_{1,\lambda}^{\text{inter}}(\mathbf{q}, i\nu_n)$ by $v_x^0(k_F)$. (That is, both the single-particle interband conductivity and the photon-phase phonon coupling are given in terms of the dimensionless function $f(\omega)$ defined in Ref. [5].) Such correlation function is finite indeed and is of the same order as the expression (32). However, when analyzing complicated CDW systems, this approximation has to be taken with reservation.

VI. CONCLUSION

In this article, we have derived the infrared selection rules for the single-particle and collective contributions to the optical conductivity in the tetramerized CDW system with the electron-phonon coupling related to the variations of electron site energies. We have shown that the relations between the effective numbers of charge carriers and the activation energy of transport coefficients, or the MIR optical threshold energy, observed in the ordinary Peierls systems are naturally explained in terms of the CDW coherence effects. The same coherence effects are expected to be important in the correlated multiband systems with the CDW instability, as well. The quantitative analysis of the latter systems is left for future investigations.

Acknowledgement

This research was supported by the Croatian Ministry of Science and Technology under Project 119-1191458-0512.

APPENDIX A: VERTEX FUNCTIONS AND CORRELATION FUNCTIONS IN THE TETRAMERIZED Q1D ELECTRONIC SYSTEM

In order to fix the notation, here we rewrite the textbook expressions [5, 6, 7, 8] for the exactly solvable tetramerized CDW case in which the electron-phonon coupling is independent of the electron wave vectors (Eq. (2) in the main text).

The total Hamiltonian reads as $H = H_0 + H'_1$, with the bare Hamiltonian and the electron-phonon coupling Hamiltonian given, respectively, by

$$\begin{aligned} H_0 &= \sum_{\mathbf{k}\sigma} \varepsilon(\mathbf{k}) c_{\mathbf{k}\sigma}^\dagger c_{\mathbf{k}\sigma} + \frac{1}{2M} \sum_{l=\pm 1} \sum_{\mathbf{q}\approx 0} \left[p_{\mathbf{q}+l\mathbf{Q}}^\dagger p_{\mathbf{q}+l\mathbf{Q}} \right. \\ &\quad \left. + (M\omega_{\mathbf{q}+l\mathbf{Q}}^0)^2 u_{\mathbf{q}+l\mathbf{Q}}^\dagger u_{\mathbf{q}+l\mathbf{Q}} \right], \\ H'_1 &= \sum_{\mathbf{q}\approx 0\mathbf{k}\sigma} \left[\frac{g e^{i\phi}}{\sqrt{N}} (u_{A\mathbf{q}} + i u_{\varphi\mathbf{q}}) c_{\mathbf{k}+\mathbf{q}\sigma}^\dagger c_{\mathbf{k}+\mathbf{Q}\sigma} + \text{H.c.} \right]. \end{aligned} \quad (\text{A1})$$

Here $\varepsilon(\mathbf{k}) = -\sum_\alpha 2t_\alpha \cos k_\alpha a_\alpha$ is the bare electron dispersion. $p_{\mathbf{q}+l\mathbf{Q}}$ is the phonon field conjugate to $u_{\mathbf{q}+l\mathbf{Q}}$ and $\omega_{\mathbf{q}+l\mathbf{Q}}^0$ is the bare phonon frequency.

The result of the phase transformation of H , which leads to the replacement $u_{A\mathbf{q}} \rightarrow \delta_{\mathbf{q},0} \langle u_A \rangle + u_{A\mathbf{q}}$, is the effective tetramerized single-electron Hamiltonian

$$\tilde{H}_0^e = \sum_{l\mathbf{k}\sigma} H_0^{ll}(\mathbf{k}) c_{l\mathbf{k}\sigma}^\dagger c_{l\mathbf{k}\sigma}, \quad (\text{A2})$$

with the index $l = -1, 0, 1, 2$, and with $\sum_{\mathbf{k}}$ running over the first Brillouin zone of the tetramerized lattice. The matrix elements in the Hamiltonian (A2) are $H_0^{ll}(\mathbf{k}) = \varepsilon_l(\mathbf{k}) = \varepsilon(\mathbf{k}+l\mathbf{Q})$, representing the dispersions of four artificially tetramerized bands, and $H_0^{l+1}(\mathbf{k}) = \Delta \exp\{i\phi\}$, with $\Delta = g \langle u_A \rangle / \sqrt{N}$ being the interband hybridization term. The diagonalization of (A2) leads to

$$\tilde{H}_0^e = \sum_{L\mathbf{k}\sigma} E_L(\mathbf{k}) c_{L\mathbf{k}\sigma}^\dagger c_{L\mathbf{k}\sigma}. \quad (\text{A3})$$

The $E_L(\mathbf{k})$ are four Bloch energies of the present problem (Eqs. (4) in the main text), and they, together with the total energy of the electronic system, depend on the phase ϕ in $H_0^{l+1}(\mathbf{k})$.

The observation (see the discussion of Fig. 1 in Sec. 2.1) that, for $\langle u_A \rangle \neq 0$, the lattice vibrations associated with $u_{A\mathbf{q}}$ and $u_{\varphi\mathbf{q}}$ are Raman and infrared active, respectively, means that there will be the direct photon-phonon coupling similar to the photon-phonon coupling in ordinary semiconductors. In principle, one can also expect the electron-mediated photon-phonon coupling, and, as discussed in detail in Sec. 5, in the common microscopic approaches, exactly this coupling is regarded as the dominant coupling [5, 6, 7, 8]. It is given in terms of the

dimensionless electron-phonon coupling constants, $g_\lambda^{L'L}(\mathbf{k}_+, \mathbf{k})$ in

$$\tilde{H}_1 = \sum_{\lambda \mathbf{q} \approx 0} u_{\lambda \mathbf{q}} \sum_{LL' \mathbf{k} \sigma} \frac{g}{\sqrt{N}} g_\lambda^{L'L}(\mathbf{k}_+, \mathbf{k}) c_{L' \mathbf{k} + \mathbf{q} \sigma}^\dagger c_{L \mathbf{k} \sigma}, \quad (\text{A4})$$

and the electron-photon coupling constants (current vertices).

The coupling constant $g_\lambda^{L'L}(\mathbf{k}_+, \mathbf{k})$ in Eq. (A4) is given in the usual way

$$g_\lambda^{L'L}(\mathbf{k}_+, \mathbf{k}) = \sum_l [e^{i\phi_\lambda} U_{\mathbf{k}+\mathbf{q}}(l, L') U_{\mathbf{k}}^*(l+1, L) + e^{-i\phi_\lambda} U_{\mathbf{k}+\mathbf{q}}(l+1, L') U_{\mathbf{k}}^*(l, L)] \quad (\text{A5})$$

($\mathbf{k}_+ = \mathbf{k} + \mathbf{q}$). Here $\phi_A = \phi$ and $\phi_\varphi = \phi + \pi/2$ are two useful abbreviations. The $U_{\mathbf{k}}(l, L)$ are the transformation-matrix elements defined by

$$c_{\mathbf{k}+l \mathbf{Q} \sigma}^\dagger \equiv c_{l \mathbf{k} \sigma}^\dagger = \sum_L U_{\mathbf{k}}(l, L) c_{L \mathbf{k} \sigma}^\dagger. \quad (\text{A6})$$

The coupling of electrons to external long-wavelength scalar fields has the form which is similar to Eq. (A4),

$$H^{\text{ext}} = \sum_{\mathbf{q}} V^{\text{ext}}(-\mathbf{q}) \sum_{LL' \mathbf{k} \sigma} e q^{LL'}(\mathbf{k}_+, \mathbf{k}) c_{L' \mathbf{k} + \mathbf{q} \sigma}^\dagger c_{L \mathbf{k} \sigma}. \quad (\text{A7})$$

Here the $q^{L'L}(\mathbf{k}_+, \mathbf{k})$ are the dimensionless monopole-charge vertices, in the intraband channel equal to unity, and in the interband channel proportional to the interband current vertex $J_\alpha^{L'L}(\mathbf{k})$,

$$q^{L'L}(\mathbf{k}_+, \mathbf{k}) = \sum_l U_{\mathbf{k}+\mathbf{q}}(l, L') U_{\mathbf{k}}^*(l, L) \quad (\text{A8})$$

$$\approx \delta_{L, L'} + (1 - \delta_{L, L'}) \sum_\alpha \frac{(\hbar/e) q_\alpha J_\alpha^{L'L}(\mathbf{k})}{E_{L'}(\mathbf{k}_+) - E_L(\mathbf{k})},$$

with $\mathbf{q} = \sum_\alpha q_\alpha \hat{e}_\alpha$.

Finally, after neglecting the relaxation processes in the electron-hole propagators associated with the disorder in the system, the renormalization of the phonon frequencies in (A1) is given in terms of the phonon self-energy

$$\hbar \Pi_\lambda(\mathbf{q}, i\nu_n) = g^2 V_0 \chi_{\lambda, \lambda}(\mathbf{q}, i\nu_n), \quad (\text{A9})$$

where the correlation function $\chi_{\lambda, \lambda}(\mathbf{q}, i\nu_n)$ has the form

$$\chi_{\lambda, \lambda}(\mathbf{q}, i\nu_n) = \frac{1}{V} \sum_{LL' \mathbf{k} \sigma} |g_\lambda^{L'L}(\mathbf{k}_+, \mathbf{k})|^2 \times \frac{f_{L'}(\mathbf{k}_+) - f_L(\mathbf{k})}{i\hbar\nu_n + E_{L'}(\mathbf{k}_+) - E_L(\mathbf{k})}. \quad (\text{A10})$$

In the same approximation, the electron-mediated coupling of phonons to the external scalar fields is given by $\chi_{\lambda, 1}(\mathbf{q}, i\nu_n)$. This correlation function is obtained by replacing the vertices $|g_\lambda^{L'L}(\mathbf{k}_+, \mathbf{k})|^2$ in Eq. (A10) by $g_\lambda^{L'L}(\mathbf{k}_+, \mathbf{k}) q^{LL'}(\mathbf{k}, \mathbf{k}_+)$. Similarly, the charge-charge correlation function $\chi_{1, 1}(\mathbf{q}, i\nu_n)$ is given by Eq. (A10) with $|q^{LL'}(\mathbf{k}, \mathbf{k}_+)|^2$ being the vertices in question. For all three correlation functions we obtain $\chi_{i, j}(\mathbf{q}, \omega)$, $i, j \in \{1, \lambda\}$, by the analytical continuation of $\chi_{i, j}(\mathbf{q}, i\nu_n)$.

-
- [1] L. Forró, R. Gaál, H. Berger, P. Fazekas, K. Penc, I. Kézsmárki and G. Mihály, Phys. Rev. Lett. **85**, 1938 (2000).
- [2] S. Fagot, P. Foury-Leylekian, S. Ravy, A.-P. Pouget and H. Berger, Phys. Rev. Lett. **90**, 196401 (2003).
- [3] I. Kézsmárki, G. Mihály, R. Gaál, N. Barišić, A. Akrap, L. Forró, C.C. Homes and L. Mihály, Phys. Rev. Lett. **96**, 186402 (2006); I. Kézsmárki, G. Mihály, R. Gaál, N. Barišić, H. Berger, L. Forró, C.C. Homes and L. Mihály, Phys. Rev. B **71**, 193103 (2005).
- [4] S. Mitrovic, P. Fazekas, C. Søndergaard, D. Ariosa, N. Barišić, H. Berger, D. Cloötta, L. Forró, H. Höchst, I. Kupčić, D. Pavuna and G. Margaritondo, Phys. Rev. B **75**, 153103 (2007).
- [5] P.A. Lee, T.M. Rice and P.W. Anderson, Solid State Commun. **14**, 703 (1974).
- [6] H.J. Schulz, Phys. Rev. B **18**, 5756 (1978).
- [7] T.M. Rice, P.A. Lee and M.C. Cross, Phys. Rev. B **20**, 1345 (1979).
- [8] G. Grüner, *Density Waves in Solids* (Addison-Wesley, New York, 1994), and references therein.
- [9] H. Fukuyama, J. Phys. Soc. Japan **41**, 513 (1976); H. Fukuyama and P.A. Lee, Phys. Rev. B **17**, 535 (1978).
- [10] S.A. Brazovskii, I.E. Dzyaloshinskii and S.P. Obukhov, Zh. Eksp. Teor. Fiz. **72**, 1550 (1977) (Sov. Phys. JETP **45**, (1977) 814).
- [11] P.B. Littlewood, Phys. Rev. B **36**, 3108 (1987).
- [12] S.N. Artemenko and A.F. Volkov, in *Charge Density Waves in Solids*, Eds. L.P. Gor'kov and G. Grüner (Elsevier, Amsterdam, 1989) p. 365.
- [13] K. Maki and A. Virosztek, Phys. Rev. B **41**, 557 (1990).
- [14] S.A. Brazovskii, J. Phys. I **3**, 2417 (1993).
- [15] J. Sólyom, Adv. Phys. **28**, 209 (1979).
- [16] T. Giamarchi, Phys. Rev. B **44**, 2905 (1991); T. Giamarchi, *Quantum Physics in 1D* (Clarendon Press, Oxford, 2004).
- [17] K. Kim, R. McKenzie and J.W. Wilkins, Phys. Rev. Lett. **71**, 4015 (1993).

- [18] R. McKenzie and J.W. Wilkins, Phys. Rev. Lett. **69**, 1085 (1992).
- [19] I. Kupčić, Physica B **322**, 154 (2002).
- [20] I. Kupčić and S. Barišić, Phys. Rev. B **75**, 094508 (2007).
- [21] I. Kupčić, Physica B **344**, 27 (2004).
- [22] D. Pines and P. Nozières, *The Theory of Quantum Liquids I* (Addison-Wesley, New York, 1989).
- [23] I. Kupčić and S. Barišić, Fizika A **14**, 47 (2005).
- [24] D. Vollhardt and P. Wölfle, Phys. Rev. B **22**, 4666 (1980).
- [25] T.B. Lyngø and T.G. Pedersen, Phys. Rev. B **67**, 075206 (2003).
- [26] N.C. Banik, E.M. Conwell and C.S. Jacobsen, Solid State Commun. **38**, 267 (1981).
- [27] L. Forró, J.R. Cooper, A. Jánossy and K. Kamarás, Phys. Rev. B **34**, 9047 (1986).
- [28] L. Degiorgi, B. Alavi, G. Mihály and G. Grüner, Phys. Rev. B **44**, 7808 (1991).
- [29] G.D. Mahan, *Many-particle Physics* (Plenum Press, New York, 1990).